https://doi.org/10.5194/acp-2021-619
Preprint. Discussion started: 17 August 2021


Atmospheric Chemistry and Physics Discussions

# Land-surface forcing and anthropogenic heat modulate ozone by meteorology: A perspective from the Yangtze River Delta region

Chenchao Zhan [a], Min Xie [a,*]

[a] School of Atmospheric Sciences, CMA-NJU Joint Laboratory for Climate Prediction Studies, Jiangsu Collaborative Innovation Center for Climate Change, Joint Center for Atmospheric Radar Research of CMA/NJU, Nanjing University, Nanjing 210023, China

-------------------------------------------------------------------

[*] Corresponding author. minxie@nju.edu.cn (M. Xie)

**Abstract:** With the rapid advance in urbanization, land-surface forcing related to the urban expansion and anthropogenic heat (AH) release from human activities significantly affect the urban climate and in turn the air quality. Focusing on the Yangtze River Delta (YRD) region, a highly urbanized place with sever ozone ($O_3$) pollution and complex geography, we estimate the impacts of land-surface forcing and AH on meteorology (meteorological factors and local circulations) and $O_3$ using the WRF-chem model, which can enhance our understanding about the formation of $O_3$ pollution in those rapidly developing regions with unique geographical features as most of our results can be supported by previous studies conducted in other regions in the world. Regional $O_3$ pollution episodes occur frequently (26 times per year) in the YRD in recent years. These $O_3$ pollution episodes are usually under calm conditions characterized by high temperature (over 20 °C), low relative humidity (less than 80%), light wind (less than 3 m $s^{-1}$) and shallow cloud cover (less than 5). In this case, high $O_3$ mainly appears during the daytime influenced by the local circulations (the sea and the lake breezes). The change in land-surface forcing can cause an increase in 2-m temperature ($T_2$) by maximum 3 °C, an increase in planetary boundary layer height (PBLH) by maximum 500 m and a decrease in 10-m wind speed ($WS_{10}$) by maximum 1.5 m $s^{-1}$, and surface $O_3$ can increase by maximum 20 μg $m^{-3}$ eventually. Furthermore, the expansion of coastal cities enhances the sea-breeze below 500 m. During the advance of the sea-breeze front inland, the upward air flow induced by the front makes well vertical mixing of $O_3$. However, once the sea-breeze is fully formed, further progression inland is stalled, thus the $O_3$ removal by the low sea-breeze will be weakened and surface $O_3$ can be 10 μg $m^{-3}$ higher in the case with cities than no-cities. The

https://doi.org/10.5194/acp-2021-619
Preprint. Discussion started: 17 August 2021



expansion of lakeside cities can extend the lifetime of the lake-breeze from the noon to the afternoon. Since the net effect of the lake-breeze is to accelerate the vertical mixing in the boundary layer, the surface $O_3$ can increase as much as 30 μg $m^{-3}$ in lakeside cities. Compared with the effects from land-surface forcing, the impacts of AH are relatively small. And the changes mainly appear in and around cities where AH emission is large. There are increases in $T_2$, PBLH, $WS_{10}$ and surface $O_3$ when AH are taken into account, with the increment about 0.2 °C, 75 m, 0.3 m $s^{-1}$ and 4 μg $m^{-3}$, respectively. Additionally, AH can affect the urban-breeze circulations, meteorological factors and $O_3$ concentration, but its effect on local circulations, such as the sea and the lake breezes, seems to be limited.

**Key Words:** ozone; meteorology; local circulations; land-surface forcing; anthropogenic heat; the Yangtze River Delta;

## 1 Introduction

Ozone ($O_3$) is a key constituent in the atmosphere, and is deeply relevant to climate (Worden et al., 2008), biosphere (Van Dingenen et al., 2009) and human health (Jerrett et al., 2009). $O_3$ acts quite differently in different parts of the atmosphere, often described as being "good up high and bad nearby". $O_3$ in the stratosphere helps protect life on earth from strong ultraviolet radiation. However, high $O_3$ in the troposphere is harmful to human respiratory system and the growth of vegetation, and thereby the tropospheric $O_3$ has long been regarded as an important air pollutant (Young et al., 2013).

Tropospheric $O_3$ is a secondary air pollutant, which is formed by a series of complex chemical reactions (Chameides and Walker, 1973; Xie et al., 2014) of precursor gases such as nitrogen oxides ($NO_x$=NO+$NO_2$) and volatile organic compounds (VOCs) in combination with sunlight. The global average lifetime of tropospheric $O_3$ is 20 to 25 days, and it will be reduced to 5 days in boundary layer (Young et al., 2013). The relatively long lifetime of tropospheric $O_3$ favors regional/long-range transport, and brings huge challenges to its control (Shao et al., 2006). $O_3$ levels considerably depend on the variations in weather conditions because weather conditions play an important role in determining the chemistry, dispersion and removal of $O_3$ (Jacob and Winner, 2009). Generally, elevated $O_3$ occurs under warm dry weather with strong sunlight, high temperature, low relative humidity and light wind speed (Zhang et al., 2015). Furthermore, weather conditions can have many

https://doi.org/10.5194/acp-2021-619
Preprint. Discussion started: 17 August 2021


Atmospheric Chemistry and Physics Discussions

similarities in certain weather pattern (Buchholz et al., 2010; Zhan et al., 2019), and the main weather patterns associated with $O_3$ episodes in China are tropical cyclones and continental anticyclones (Wang et al., 2017).

$O_3$ levels as well as weather conditions in urban areas are of great concern simply because urban areas have huge populations. A report from the United Nations pointed out that 69.6% of the world's population will live in cities by 2050. The urbanization process has further increased urban environmental hazards (Zhang et al., 2011), particularly in the most rapidly developing countries like China (Liu and Tian, 2010). Because of historical and cultural factors, many cities have similar topography, usually along the coast, close to mountains or in basins. For these cities, the local circulations induced by thermal contrast of the topography, such as sea-land breezes, mountain-valley breezes and lake-land breezes, will have an important impact on air quality of the city, especially when the dominant background weather system is weak (Crosman and Horel, 2010). Examples can be found around the world. Ding et al. (2004) simulated the main features of the sea-land breezes during a multiday episode in the Pearl River Delta (PRD) region, and found that the sea-land breezes play a crucial role in transporting air pollutant between inland and coastal cities. Miao et al. (2015) studied the effects of mountain-valley breezes on boundary layer structure in the Beijing-Tianjin-Hebei (BTH) region, suggesting that the mountain-valley breezes are vital to the vertical transport and distribution of air pollutants in Beijing. Wentworth et al. (2015) identified a causal link between lake-breeze and $O_3$ in the Greater Toronto Area that the daytime $O_3$ maxima was 13.6-14.8 ppb higher on lake breeze days than no-lake breeze days.

The land-surface forcing and anthropogenic heat (AH) of a city also affect the atmospheric state and compositions above it (Yu et al., 2012; Oke et al., 2017). The land-surface forcing changes chiefly come from the urban expansion (typically from vegetation to impervious surface), which directly changes the surface physical properties (e.g., albedo, surface moisture and roughness) and thereby significantly affects the meteorology and in turn the air quality. Li et al. (2019) found that increases in thermal inertia, surface roughness and evapotranspiration due to urban expansion can lead to an increase in $O_3$ by up to 5.6 ppb in Southern California. AH is an important waste by-product of urban metabolism. Nearly all energy consumed by human activities will be dissipated as heat within Earth's land-atmosphere system (Flanner, 2009; Sailor, 2011) that is then "injected" into the energy balance processes. Ryu et al. (2013a) reported that AH affects the

https://doi.org/10.5194/acp-2021-619
Preprint. Discussion started: 17 August 2021




characteristics/structures of boundary layer and local circulations, resulting in an increase of $O_3$ by 3.8 ppb in the Seoul metropolitan area.

These previous studies separately investigated the impact of local circulations, land-surface forcing and AH on meteorology and air quality, usually focusing on a specific megacity. However, local circulations, land-surface forcing and AH can work together in near-calm conditions. And the role of multi-scale atmospheric circulations associated with the abovementioned factors in regional meteorology and air quality of city clusters is unclear. Actually, complex interactions exist widely among these thermally-driven circulations and the effects can even spread from one city to nearby areas. For example, Zhu et al. (2015) demonstrated that the meteorological conditions and air quality over Kunshan are significantly affected by Shanghai urban land surface forcing (Kunshan is located downstream of Shanghai, with a straight-line distance of about 50 km). Therefore, assessing the effects of land-surface forcing and AH (The topography rarely changes.) in the city cluster is meaningful, which helps understand the connection between urban development, local meteorology and regional air quality.

The Yangtze River Delta (YRD) region, located on the western coast of the Pacific Ocean (Figure 1a), has undergone accelerated urbanization process and rapid economic development over the past decades, and is now one of the largest economic zones in the world. It includes the areas of the southern part of Jiangsu Province, the northern part of Zhejiang Province and the eastern part of Anhui Province, with 26 mega/large cities such as Shanghai, Hangzhou and Nanjing (Figure 1b). With dense population and huge energy consumption, this area is now suffering from air quality deterioration (Ding et al., 2013; Xie et al., 2017), especially severe $O_3$ pollution in recent years (Zhan et al., 2020, 2021). It was reported that 16 out of the 26 typical cities in the YRD failed to meet the urban national standard for $O_3$ in 2017 (Bulletin on the state of China's ecological environment in 2018, http://www.cleanairchina.org/ product/9943.html), and to make matters worse, $O_3$ concentration has been rising in this region during the past few years (Li et al., 2020; Wang et al., 2020). The YRD region is deeply affected by the East Asian monsoon, and has complex weather like other mid-latitude regions in the world. Sever air pollution and unique geography make this area an ideal place for studying the complex interactions between the atmosphere and human activities.

In this study, the impacts of land-surface forcing and AH on meteorology in the central YRD

https://doi.org/10.5194/acp-2021-619
Preprint. Discussion started: 17 August 2021

Atmospheric Chemistry and Physics Discussions
Open Access

region, and how these impacts further modulate $O_3$ are investigated using the Weather Research and Forecasting model coupled to Chemistry (WRF-Chem). These results fill the knowledge gap about the formation of $O_3$ pollution in this region and provide valuable insight for other rapidly developing regions with complex geography in the world. The remainder of this paper is organized as follows. Sect. 2 gives a detailed description about the observation data, the model setup and experimental design. The main results, including the characteristics of $O_3$ pollution episodes, the model evaluation and the response of $O_3$ to land-surface forcing and AH, are presented in Sect. 3. Summary and conclusions are given in Sect. 4.

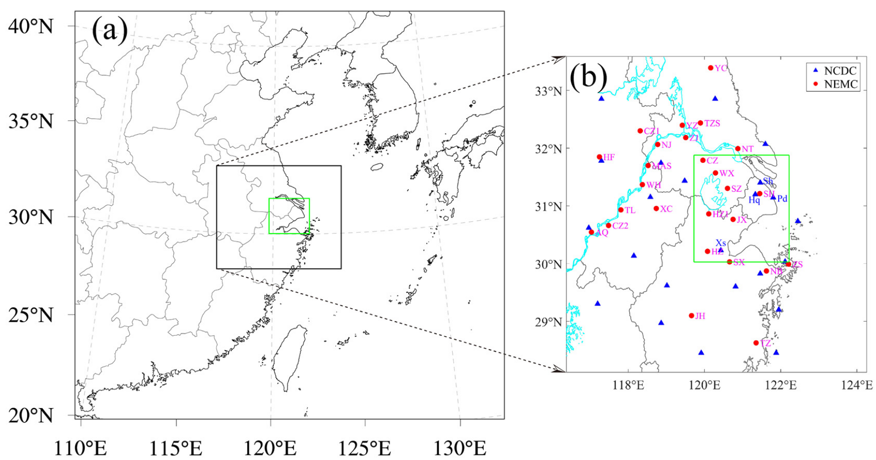


**Figure 1.** (a) Three nested WRF-Chem domains, (b) the locations of 26 cities (red dots) and weather stations (blue triangles) in the YRD. The green rectangular regions represent the innermost domain and also the central YRD region. These cities in (b) include: the megacity Shanghai (SH); Hangzhou (HZ), Ningbo (NB), Jiaxing (JX), Huzhou (HZ1), Shaoxing (SX), Jinhua (JH), Zhoushan (ZS) and Taizhou (TZ) located in Zhejiang Province; Nanjing (NJ), Wuxi (WX), Changzhou (CZ), Suzhou (SZ), Nantong (NT), Yancheng (YC), Yangzhou (YZ), Zhenjiang (ZJ) and Taizhoushi (TZS) located in Jiangsu Province; and Hefei (HF), Wuhu (WH), Maanshan (MAS), Tongling (TL), Anqing (AQ), Chuzhou (CZ1), Chizhou (CZ2) and Xuancheng (XC) located in Anhui Province.

## 2 Materials and methods

https://doi.org/10.5194/acp-2021-619
Preprint. Discussion started: 17 August 2021



## 2.1 Surface observations

Hourly $O_3$ concentrations monitored by the National Environmental Monitoring Center (NEMC) of China are used in this study. These data strictly follow the national monitoring standards HJ 654-2013 and HJ 193-2013 (http://www.cnemc.cn/jcgf/dqhj/), and can be available at https://quotsoft.net/air/, a mirror of data from the official NEMC real-time publishing platform (http://106.37.208.233:20035/). The nationwide observation network initially operated in 74 major cities in 2013, and it has grown to more than 1,500 stations covering 454 cities by 2017 (Lu et al., 2018). The urban hourly $O_3$ concentrations are average results of measurements at all monitoring sites for each city. The maximum daily 8-h running average (MDA8) $O_3$ concentrations are then calculated based on the hourly $O_3$ concentration with more than 18-h measurements in the day (Liao et al., 2017).

Meteorological data are provided by the National Climatic Data Center (NCDC), including temperature, wind speed and direction, and relative humidity, etc. These data as well as the technical documents recording the quality control, data collection and archive can be available at ftp://ftp.ncdc.noaa.gov/pub/data/noaa/isd-lite/. Locations of surface observation stations are shown in Figure 1b. Specifically, the meteorological stations in the innermost domain include Pudong (Pd), Shanghai (Sh), Hongqiao (Hq) and Xiaoshan (Xs).

## 2.2 MODIS-based and USGS land use classifications

To investigate the impact of land-surface forcing on regional meteorology and $O_3$ evolution in the YRD, the two land use categories defaulted in WRF (MODIS-based and USGS land use classifications) are used to set up the first two sensitivity simulations (Table 2). The MODIS-based land cover product was created from 500-m MODIS Terra and Aqua satellite imagery (Friedl et al., 2010), and replaced USGS as the default settings in WRF since version 3.8. The USGS data primarily derived from the Advanced Very High Resolution Radiometer (AVHRR) from 1992 to 1993 at 1-km spatial resolution (Loveland et al., 2000), which is much earlier than the MODIS data. Figure 2 presents the land cover maps in the innermost domain. Apparently, urban fraction with MODIS is much higher than USGS, indicating rapid urbanization in recent decades in the YRD. The differences in urban land-surface forcing between USGS and MODIS mainly depend on urban expansion. Additionally, the Finer Resolution Observation and Monitoring-Global Land Cover in 2015 (From-GLC_2015), which can be considered as one of the latest (2015) and finest (30-m) land

https://doi.org/10.5194/acp-2021-619
Preprint. Discussion started: 17 August 2021



cover datasets (Gong et al., 2019), is quite consistent with the performance of MODIS in this region. This further confirms that urban fraction with MODIS is close to the reality.

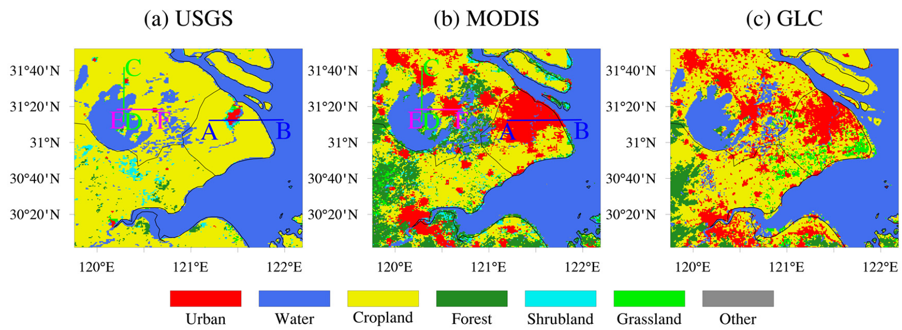


**Figure 2.** Land cover maps in the innermost domain, including the result of (a) USGS, (b) MODIS, and (c) From-GLC_2015.

### 2.3 Anthropogenic heat flux modeling

Another simulation involved the urban canopy model with the gridded AH fluxes is conducted to estimate AH release in the central YRD. The AH fluxes are mainly the result of chemical energy or electrical energy that are converted to heat, thereby they can be quantified using the top-down energy inventory method. Based on the statistics data of energy consumption in 2016, the AH fluxes were calculated, and then were grided as 144 rows and 144 columns with a resolution at 2.5 arcmin using population density in China. Details on the calculation as well as the distribution of AH fluxes, and how to add AH fluxes into the urban canopy can refer to Xie et al. (2016a, b). Figure 3 gives the spatial distribution of AH fluxes in the innermost domain. In the urban areas, the AH fluxes usually exceed 20 W m$^{-2}$. Some big cities, like Shanghai, can have a value of AH flux as high as 200 W m$^{-2}$. Except for the urban areas, the AH fluxes are generally less than 5 W m$^{-2}$ in most parts of the YRD region. In particular, in those places where there is no human activity, the AH flux is 0.

https://doi.org/10.5194/acp-2021-619
Preprint. Discussion started: 17 August 2021



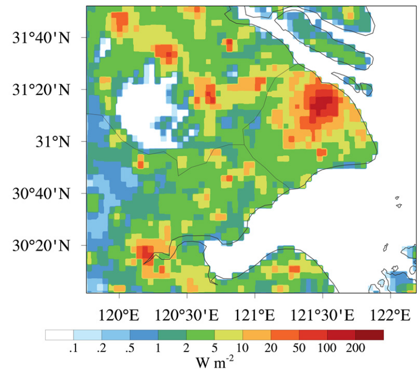


**Figure 3.** Spatial distribution of anthropogenic heat fluxes in the innermost domain.

## 2.4 Model set-up and experimental designs

The WRF-Chem model is a fully coupled online numerical weather prediction model with chemistry component (Grell et al., 2005), in which air quality and the meteorological component use the same coordinates, transport schemes and physics schemes in space and time. In this study, the WRF-Chem version 3.9.1 is applied. The initial and boundary conditions of meteorological fields are from the National Centers for Environmental Prediction (NCEP) global final analysis fields every 6 h with a spatial resolution of 1° × 1°. There are 32 vertical levels extending from the surface to 100 hPa with 12 levels located below 2 km to resolve the boundary layer processes. Furthermore, the domain and options for physical and chemical parameterization schemes are summarized in Table 1. The anthropogenic emissions are provided by the Multiresolution Emission Inventory for China (MEIC) in 2017 with a resolution of 0.25° (http://meicmodel.org/), which includes 10 air pollutants and $CO_2$ from power, industry, residential, transportation and agriculture sectors. The biogenic emissions are estimated online by the Model of Emissions of Gases and Aerosols from Nature (MEGAN) in WRF-Chem (Guenther et al., 2006).

**Table 1.** The domains and major options for WRF-Chem

| Items | Contents |
|---|---|
| Dimensions (x, y) | (101, 96), (146, 121), (236, 206) |
| Grid spacing (km) | 25, 5, 1 |

https://doi.org/10.5194/acp-2021-619
Preprint. Discussion started: 17 August 2021

Atmospheric Chemistry and Physics Discussions
Open Access

| | |
|---|---|
| Time step (s) | 75 |
| Microphysics | Purdue Lin microphysics scheme (Chen and Sun, 2002) |
| Longwave radiation | RRTM scheme (Mlawer et al., 1997) |
| Shortwave radiation | Goddard scheme (Kim and Wang, 2011) |
| Surface layer | Revised MM5 Monin-Obukhov scheme |
| Land-surface layer | Noah land-surface model (Chen and Dudhia, 2001) |
| Planetary boundary layer | YSU scheme (Hong et al., 2006) |
| Cumulus parameterization | Grell 3D ensemble scheme (Grell and Devenyi, 2002) |
| Gas-phase chemistry | RADM2 (Stockwelll et al., 1990) |
| Photolysis scheme | Fast-J photolysis (Fast et al., 2006) |
| Aerosol module | MADE/SORGAM (Schell et al., 2001) |

As shown in Table 2, three numerical experiments are performed to study the effects of land-surface forcing and AH on meteorology and $O_3$ in the YRD. The MODIS_noAH experiment is a control simulation with commonly used settings. Compared with MODIS_noAH, USGS_noAH selects the USGS data at run-time through the geogrid program. Thus, the difference between the modeling results of MODIS_noAH and USGS_noAH can illustrate the changes caused by land cover. As for the impact of AH, it can be identified by comparing the modeling results of MODIS_withAH and MODIS_noAH. All three simulations run from 00:00 on 21 May to 00:00 on 4 June in 2017 with the first 88 h as spin-up time, using the same physical and chemical parameterization schemes (Table 1).

**Table 2.** The three numerical experiments.

| Cases | Land use categories | Whether to add AH |
|---|---|---|
| MODIS_noAH | MODIS-based | No |
| USGS_noAH | USGS | No |
| MODIS_withAH | MODIS-based | Yes |

**2.5 Model evaluation**

https://doi.org/10.5194/acp-2021-619
Preprint. Discussion started: 17 August 2021



The simulation results in the innermost domain, including $O_3$ concentration, 2-m air temperature ($T_2$), relative humidity (RH), 10-m wind speed ($WS_{10}$) and 10-m wind direction ($WD_{10}$) are examined against the surface observations described in Sect. 2.1. The statistical metrics, including the mean bias (MB), root mean square error (RMSE) and correlation coefficient (COR), are used to evaluate the model performance. They are defined as follows:

$$MB = \frac{1}{N}\sum_{i=1}^{N}(\mathrm{S}_i - \mathrm{O}_i), \tag{1}$$

$$RMSE = \sqrt{\frac{1}{N}\sum_{i=1}^{N}(\mathrm{S}_i - \mathrm{O}_i)^2}, \tag{2}$$

$$COR = \frac{\sum_{i=1}^{N}(\mathrm{S}_i - \overline{\mathrm{S}})(\mathrm{O}_i - \overline{\mathrm{O}})}{\sqrt{\sum_{i=1}^{N}(\mathrm{S}_i - \overline{\mathrm{S}})^2}\sqrt{\sum_{i=1}^{N}(\mathrm{O}_i - \overline{\mathrm{O}})^2}}, \tag{3}$$

where $S_i$ and $O_i$ are the simulations and observations, respectively. N is the total amount of valid data, and $\overline{\mathrm{S}}$ and $\overline{\mathrm{O}}$ represent the average of simulations and observations, respectively. Generally, the model performance is acceptable if the values of MB and RMSE are close to 0, and that of COR is close to 1 (Xie et al., 2016a, b; Zhan et al., 2020).

## 3 Results and discussions

### 3.1 Regional $O_3$ pollution episodes in the YRD

Under adverse weather conditions, $O_3$ pollution episodes occur frequently in the YRD (Gao et al., 2020; Zhan et al., 2021). Sometimes, $O_3$ pollution can spread throughout the YRD and cause regional $O_3$ pollution, affecting an area of up to 3.5 million square kilometers and harming more than 200 million people. Based on the surface $O_3$ observations, we define the regional $O_3$ pollution in the YRD as when more than half of the 26 typical cities in the YRD fail to meet the national $O_3$ standard (In China, the national ambient air quality standard for MDA8 $O_3$ is 160 μg $m^{-3}$), and then sort out all regional $O_3$ pollution episodes and the corresponding weather patterns from 2015 to 2019 (Table S1). There were 20, 19, 34, 28 and 30 regional $O_3$ pollution cases in the YRD from 2015 to 2019, respectively. These cases mainly occurred in April to October of each year, and were usually related to high pressure, uniform pressure field and typhoon activity.

https://doi.org/10.5194/acp-2021-619
Preprint. Discussion started: 17 August 2021



Figure 4 further displays the monthly distribution of meteorological factors during the day (from 8:00 to 20:00 local time) when regional $O_3$ pollution occurs in the YRD. All the variables show significant monthly variations. The highest (lowest) temperature is found in July (April), and the relative humidity is highest in June. This may be related to the Meiyu in June, and the hot weather in July as the YRD is usually dominated by the western Pacific subtropical high after Meiyu. As for the cloud cover, the sky is covered with fewer clouds in October than other months. In addition, southeast wind prevails in the YRD from April to October under the influence of monsoon climate. As shown in Figure 4, $O_3$ pollution episodes are likely to occur in the YRD on days when the temperature exceeds 20 ℃ (Figure 4b), the relative humidity is less than 80% (Figure 4c), the cloud cover is less than 5 (Figure 4d), and the wind speed is less than 3 m $s^{-1}$ (Figure 4e). Interestingly, the local circulations induced by thermal differentiation is clearest when in absence of clouds, radiative heating is strongest and wind is weakest. Thus, both $O_3$ pollution and local circulations tend to appear in calm conditions characterized by high temperature, cloudless sky and weak wind, and the local circulation will inevitably have an impact on the distribution of $O_3$ in this case.

https://doi.org/10.5194/acp-2021-619
Preprint. Discussion started: 17 August 2021


Atmospheric Chemistry and Physics
Discussions
Open Access
EGU

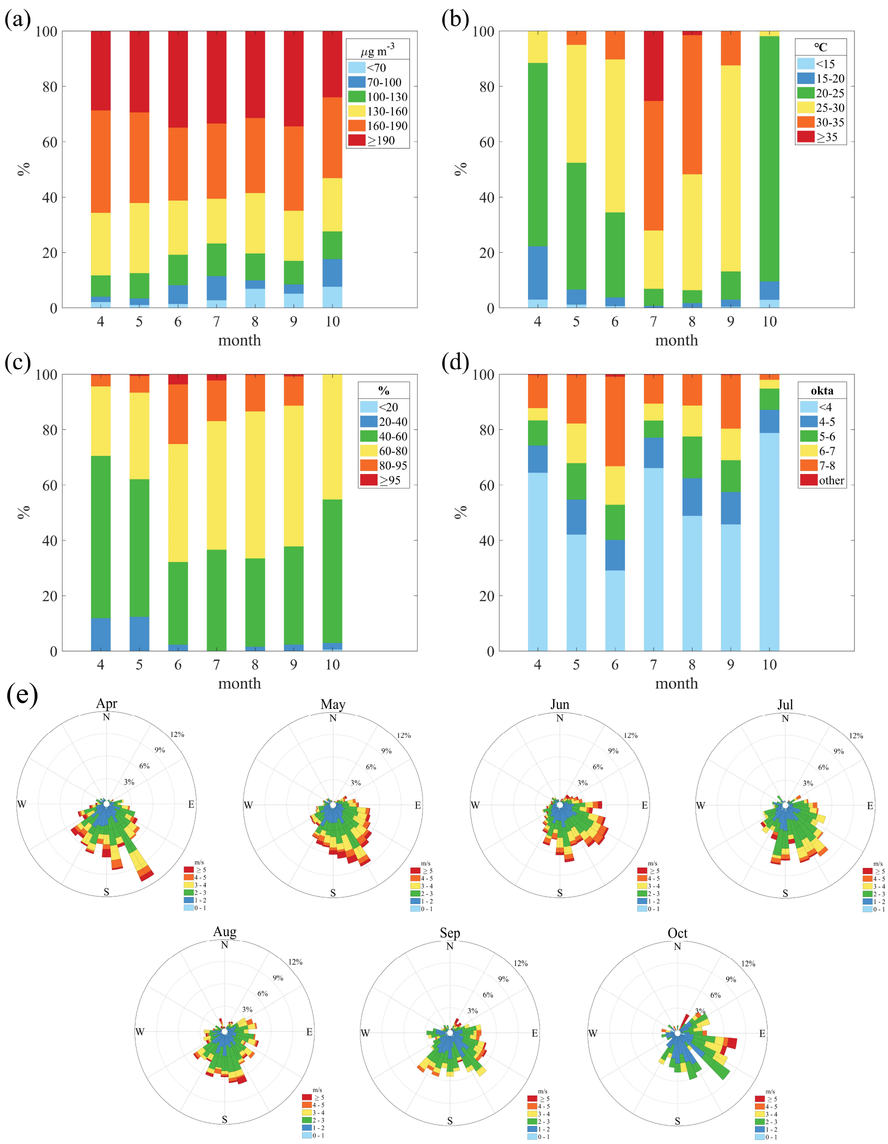


**Figure 4.** The monthly distribution of (a) $O_3$, (b) temperature, (c) relative humidity, (d) cloud cover, and (e) wind speed and direction during the daytime (8:00 to 20:00 LT) when regional $O_3$ pollution occurs in the YRD.

## 3.2 Case selection

### 3.2.1 Case for $O_3$ pollution episode

https://doi.org/10.5194/acp-2021-619
Preprint. Discussion started: 17 August 2021



For simplicity but without loss of generality, the longest-lasting regional $O_3$ pollution case in Table S1 is selected to investigate the impacts of land-surface forcing and AH on meteorology and $O_3$ pollution in the YRD. This 10-day regional $O_3$ pollution episode occurred from 25 May to 3 June in 2017. During this period, an average of 18 out of the 26 cities experienced $O_3$ pollution every day, and the MDA8 $O_3$ concentrations ranged from 168.1 to 205.1 μg $m^{-3}$. Moreover, the daily maximum air temperature ranged from 28.5 to 33.9 ℃ over the central YRD (the innermost domain) under high pressure/uniform pressure field (Figure S1). This case meets the requirements of calm weather and high $O_3$ concentration. And the relatively long duration also provide a representative result.

**3.2.2 Evaluation of model performance**

In this study, three numerical experiments are conducted using WRF-Chem (Sect. 2.4) during the period of the previously mentioned $O_3$ episode. The simulation results are validated in the innermost domain by comparing with the observational data. Table 5 presents the statistical metrics in meteorological variables that includes 2-m air temperature ($T_2$), relative humidity (RH), 10-m wind speed ($WS_{10}$) and direction ($WD_{10}$). Figure 5 further illustrates time series comparisons between these meteorological factors and their modeling results. $T_2$ is reasonably well simulated as the mean CORs (the mean of all the sites) are 0.875, 0.865 and 0.863 in MODIS_noAH, USGS_noAH and MODIS_AH, respectively. The small negative MBs at all sites suggest that our simulations underestimate $T_2$ to some extent, though this light underestimation is acceptable because of the small mean RMSE (2.3, 3.1 and 2.3 ℃). The mean MBs for $T_2$ in USGS_noAH, MODIS_noAH and MODIS_AH are -2.4, -1.0, and -0.8 ℃, indicting an improvement in temperature when new land use and AH are taken into account. These results can be confirmed by Figure 5a. With respect to RH, the mean CORs are 0.823, 0.753 and 0.825 for the three numerical experiments, respectively. All three simulations can well capture the diurnal variation of RH, but have different performance on different sites (Figure 5b). In USGS_noAH, RH is overestimated at all sites, especially Pudong site, and the mean MB is 11.2%. While RH is only overestimated at the two coastal sites (Pudong and Shanghai) but underestimated at other two sites (Hongqiao and Xiaoshan) in MODIS_noAH and MODIS_AH. Moreover, USGS_noAH has the highest mean RMSE of RH (16.3%), followed by MODIS_AH (12.4%) and MODIS_noAH (12.1%). As for $WS_{10}$, the modeling values are slightly overestimated at all sites in all three simulations. The overestimation of $WS_{10}$ may partly be attributed to the unresolved terrain features by the default

https://doi.org/10.5194/acp-2021-619
Preprint. Discussion started: 17 August 2021



surface drag parameterization causing an overestimation of wind speed in particular at low values (Jimenez and Dudhia, 2012). Specially, $WS_{10}$ in USGS_noAH is the most overestimated, followed by MODIS_AH and MODIS_noAH, with the mean MBs are 1.2, 1.0 and 0.8 m $s^{-1}$, respectively. Additionally, a high mean MB is found to correspond to a high mean RMSE (1.9, 1.8 and 1.7 m $s^{-1}$) in our simulations. In terms of $WD_{10}$, the model captures well the shift in wind direction during the study period (Figure 5d). Thus, our modeling results of wind speed and direction basically reflect the characteristics of wind fields. In summary, both the statistical metrics in Table 3 and time series in Figure 5 illustrate that all the numerical experiments can reflect the major characteristics of meteorological conditions during this $O_3$ pollution episode. Nevertheless, using new land-use data and adding AH can reduce the underestimation of $T_2$ and the overestimation of RH and $WS_{10}$ to some extent.

https://doi.org/10.5194/acp-2021-619
Preprint. Discussion started: 17 August 2021




**Table 3.** Statistical metrics in meteorological variables between observations and simulations.

| Variables | Site | | MODIS_noAH | | | | USGS_noAH | | | | MODIS_AH | | | |
|---|---|---|---|---|---|---|---|---|---|---|---|---|---|---|
| | | $\bar{O}$[a] | $\bar{S}$[b] | MB[c] | RMSE[d] | COR[e] | $\bar{S}$ | MB | RMSE | COR | $\bar{S}$ | MB | RMSE | COR |
| $T_2$ | Pd | 23.2 | 21.5 | -1.7 | 2.4 | 0.89 | 20.7 | -2.5 | 3.8 | 0.70 | 21.5 | -1.7 | 2.4 | 0.89 |
| (℃) | Sh | 24.6 | 23.9 | -0.7 | 2.2 | 0.87 | 22.5 | -2.1 | 2.7 | 0.90 | 24.2 | -0.5 | 2.3 | 0.84 |
| | Hq | 25.3 | 24.4 | -0.9 | 2.0 | 0.89 | 22.7 | -2.6 | 3.0 | 0.95 | 24.8 | -0.5 | 1.9 | 0.89 |
| | Xs | 25.9 | 25.1 | -0.8 | 2.4 | 0.85 | 23.8 | -2.2 | 2.8 | 0.91 | 25.5 | -0.4 | 2.4 | 0.83 |
| RH | Pd | 69.1 | 77.7 | 8.6 | 13.5 | 0.81 | 86.2 | 17.2 | 23.4 | 0.45 | 77.7 | 8.7 | 13.3 | 0.83 |
| (%) | Sh | 59.3 | 60.6 | 1.3 | 11.7 | 0.81 | 71.1 | 11.8 | 16.1 | 0.81 | 59.4 | 0.1 | 12.4 | 0.78 |
| | Hq | 59.5 | 57.7 | -1.8 | 9.8 | 0.88 | 70.6 | 11.1 | 14.5 | 0.89 | 56.2 | -3.3 | 9.8 | 0.89 |
| | Xs | 60.6 | 55.4 | -5.2 | 13.5 | 0.79 | 65.3 | 4.8 | 11.3 | 0.86 | 53.5 | -7.1 | 14.1 | 0.80 |
| $WS_{10}$ | Pd | 4.1 | 4.1 | 0.0 | 1.4 | 0.47 | 5.5 | 1.3 | 2.1 | 0.35 | 4.2 | 0.1 | 1.3 | 0.51 |
| ($m\ s^{-1}$) | Sh | 2.5 | 4.2 | 1.7 | 2.2 | 0.36 | 4.5 | 2.0 | 2.4 | 0.54 | 4.3 | 1.9 | 2.3 | 0.35 |
| | Hq | 3.7 | 3.9 | 0.2 | 1.2 | 0.54 | 3.9 | 0.2 | 1.2 | 0.53 | 4.2 | 0.5 | 1.3 | 0.50 |
| | Xs | 2.3 | 3.6 | 1.3 | 2.0 | 0.26 | 3.4 | 1.1 | 1.8 | 0.30 | 3.8 | 1.5 | 2.1 | 0.24 |
| $WD_{10}$ | Pd | 160.4 | 136.1 | -26.2 | 78.7 | 0.42 | 148.1 | -14.3 | 55.1 | 0.72 | 137.3 | -24.7 | 77.5 | 0.42 |
| (°) | Sh | 141.6 | 146.4 | 4.8 | 66.4 | 0.60 | 141.7 | 0.1 | 63.9 | 0.59 | 142.6 | 1.0 | 69.9 | 0.56 |
| | Hq | 159.7 | 140.2 | -23.4 | 80.2 | 0.46 | 153.1 | -10.6 | 74.9 | 0.52 | 142.8 | -20.4 | 91.8 | 0.29 |
| | Xs | 188.6 | 160.2 | -28.4 | 99.5 | 0.48 | 161.4 | -27.3 | 109.6 | 0.35 | 152.0 | -36.6 | 109.9 | 0.38 |

[a] $\bar{O}$ and [b] $\bar{S}$ indicate the average of observations and simulations, respectively. [c] MB indicates the mean bias, [d] RMSE indicates the root mean square error and [e] COR indicate the correlation coefficient, with statistically significant at 99% confident level.

https://doi.org/10.5194/acp-2021-619
Preprint. Discussion started: 17 August 2021


Atmospheric Chemistry and Physics
Open Access
Discussions

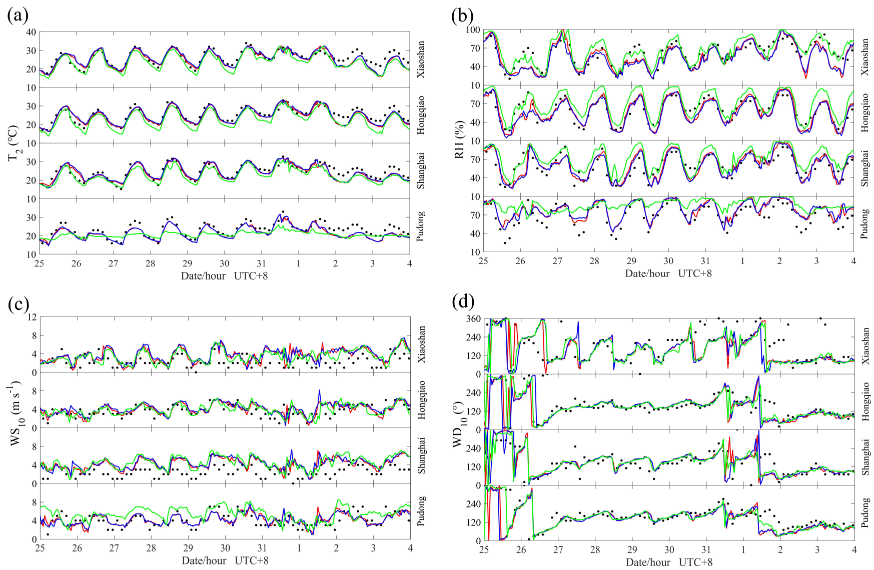


Figure 5. Time series of $T_2$, RH, $WS_{10}$ and $WD_{10}$ for observations and simulations at different meteorological stations. The black dots are the surface observations. The simulation results of MODIS_noAH, USGS_noAH and MODIS_withAH are shown in red, green and blue, respectively.

Table 4 lists the statistical metrics in $O_3$, and Figure 6 gives the hourly variations of $O_3$ for observations and simulations at different sites. With high CORs (the mean CORs are 0.80, 0.81 and 0.80 in MODIS_noAH, USGS_noAH and MODIS_AH, respectively), all the simulations can reproduce the diurnal variation of $O_3$, which shows that $O_3$ concentration reaches its maximum in the afternoon and gradually decreases to its minimum in the morning. The magnitude of $O_3$ modeling results is reasonable (Figure 6), but the peak and valley values of $O_3$ simulations are sometimes differ greatly from the observations, especially the peak value, like Huzhou. This may be related to the resolution of the emission inventory and the distribution of $O_3$ precursors. Considering the relatively low mean MB (6.9, -1.6 and 9.0 μg $m^{-3}$) and mean RMSE (49.3, 46.2 and 49.0 μg $m^{-3}$), the modeling results of $O_3$ are generally reasonable and acceptable.

**Table 4.** Statistical metrics in $O_3$ between observations and simulations.

| Case | Index | Site |
|---|---|---|

https://doi.org/10.5194/acp-2021-619
Preprint. Discussion started: 17 August 2021


| | | CZ | WX | SZ | SH | HZ1 | JX | HZ |
|---|---|---|---|---|---|---|---|---|
| | $\overline{O}$ | 89.7 | 141.8 | 121.7 | 112.8 | 95.8 | 113.2 | 104.8 |
| MODIS_noAH | $\overline{S}$ | 123.2 | 117.6 | 116.2 | 103.4 | 128.1 | 112.5 | 127.5 |
| | MB | 33.3 | -24.2 | -5.6 | -9.1 | 32.1 | -0.6 | 22.7 |
| | RMSE | 53.8 | 49.1 | 42.8 | 36.4 | 59.9 | 44.4 | 58.6 |
| | COR | 0.85 | 0.83 | 0.82 | 0.80 | 0.83 | 0.78 | 0.71 |
| USGS_noAH | $\overline{S}$ | 108.1 | 106.8 | 107.1 | 93.8 | 118.6 | 111.0 | 122.5 |
| | MB | 18.5 | -35.0 | -14.7 | -18.9 | 23.0 | -2.0 | 18.0 |
| | RMSE | 43.5 | 56.0 | 44.7 | 37.7 | 50.1 | 41.1 | 50.0 |
| | COR | 0.83 | 0.81 | 0.80 | 0.81 | 0.82 | 0.80 | 0.77 |
| MODIS_AH | $\overline{S}$ | 124.5 | 119.8 | 119.1 | 108.0 | 130.3 | 113.7 | 127.8 |
| | MB | 34.7 | -21.9 | -2.7 | -4.6 | 34.3 | 0.6 | 23.0 |
| | RMSE | 53.5 | 47.3 | 42.4 | 37.4 | 59.4 | 44.7 | 58.2 |
| | COR | 0.84 | 0.83 | 0.81 | 0.80 | 0.82 | 0.78 | 0.71 |

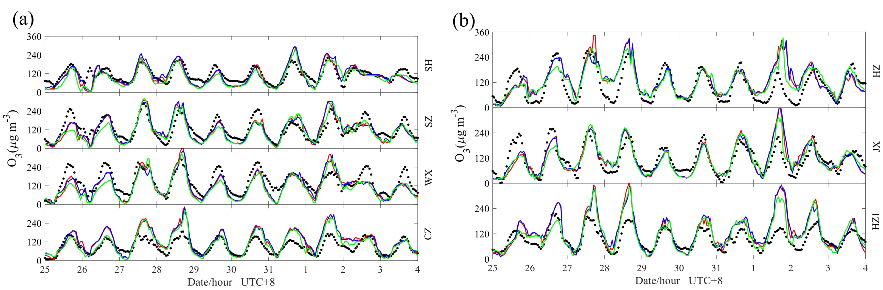


Figure 6. Same as Figure 5, but for $O_3$.

Above all, the WRF-Chem model using our configuration has a good capability in simulating the meteorology and $O_3$ air quality over the studied region in this study. It is still noteworthy that the object of inter-comparison between the three numerical experiments is not to determine which setting is most skillful in reproducing the observations. Rather, it is to diagnose and understand the differences induced by land-surface forcing and AH, and then to provide valuable insight into the formation of the $O_3$ pollution episodes.

### 3.3 Overall behaviors of $O_3$ and local circulations

Based on the results of the control simulation (MODIS_noAH), we first give an overall behavior of $O_3$ and local circulations during the study period. And then the differences induced by land-surface forcing and AH are discussed via intercomparisons between the numerical experiments.

https://doi.org/10.5194/acp-2021-619
Preprint. Discussion started: 17 August 2021




Thereby, only difference plots between USGS_noAH/MODIS_withAH and MODIS_noAH are shown in this paper, but the corresponding original plots for USGS_noAH and MODIS_withAH can be found in supplementary materials (Figure S2-5).

**3.3.1 Spatiotemporal variations of $O_3$**

As show in Figure 7, $O_3$ concentration began to rise around 8:00 local time (LT = UTC + 8 h) after sunrise, and became noticeable after only 3 hours (Figure 7a and h). During this stage, the nocturnal residual layer vanished due to the development of the convective boundary layer (Figure 8). The $O_3$-rich air mass in the residual layer was mixed with the $O_3$-poor air mass on the ground, which enhanced the surface $O_3$ in the morning (Hu et al., 2018). Around 11:00 LT, the convective boundary layer was established, and high $O_3$ produced by photochemical reactions appeared over the central YRD and persisted until 18:00 LT (Figure 7b, 7c and 8). The maximum $O_3$ production was in the middle of the boundary layer (~800 m) instead of at the surface (Figure 8). After sunset, surface $O_3$ concentrations decreased sharply due to nitrogen oxide (NO) titration. The loss of $O_3$ caused by NO titration almost ceased around 2:00 LT when $O_3$ was at its lowest level of the day (Figure 7f and g). In general, $O_3$ has a typical diurnal variation with high concentration in the daytime and low concentration at night. This is consistent with the results in Figure 6, and this rule of $O_3$ can be applied to most parts of the world. Therefore, the situation during the daytime (We select 11:00, 14:00, 17:00 and 20:00 LT in this study) should be paid attention to when it comes to $O_3$ pollution.

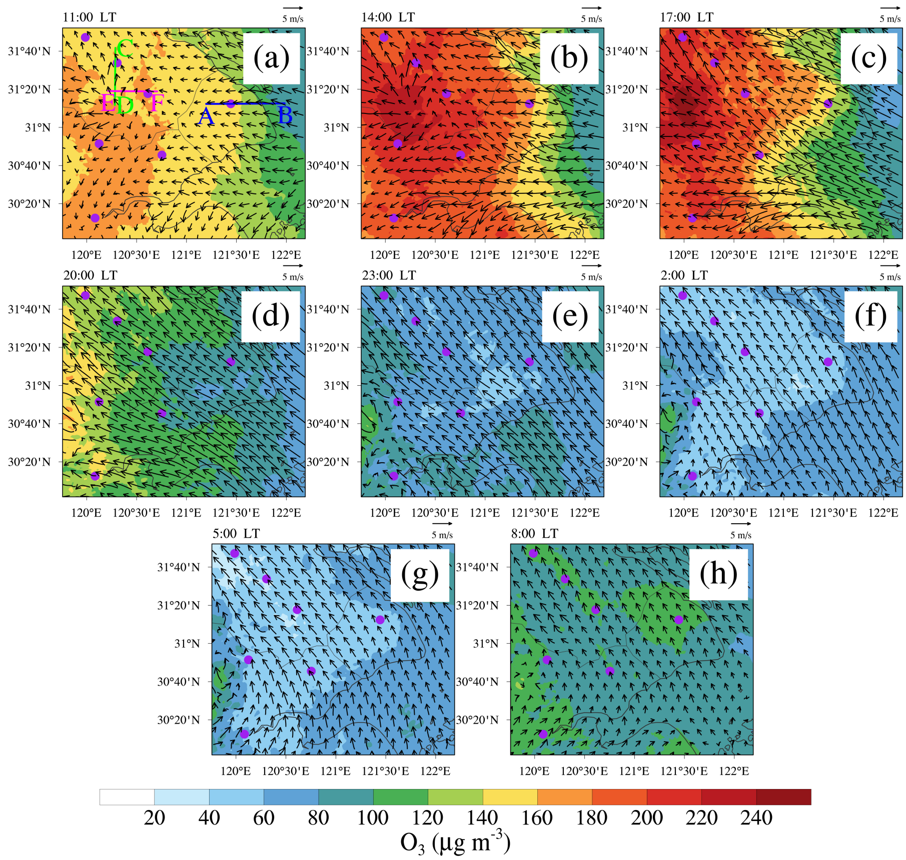


**Figure 7.** Horizontal distributions of $O_3$ and wind at the lowest model level in MODIS_noAH. (a), (b), (c) and (d) are the results at 11:00, 14:00, 17:00 and 20:00 LT, referring to the daytime. (e), (f), (g) and (h) are the results at 23:00, 2:00, 5:00 and 8:00 LT, referring to the night. The purple dots represent the locations of cities (red dots in Figure 1b) in the innermost domain. To obtain general feature, all results are the average of the study period, and the same for the subsequent results.

https://doi.org/10.5194/acp-2021-619
Preprint. Discussion started: 17 August 2021


Atmospheric Chemistry and Physics
Discussions

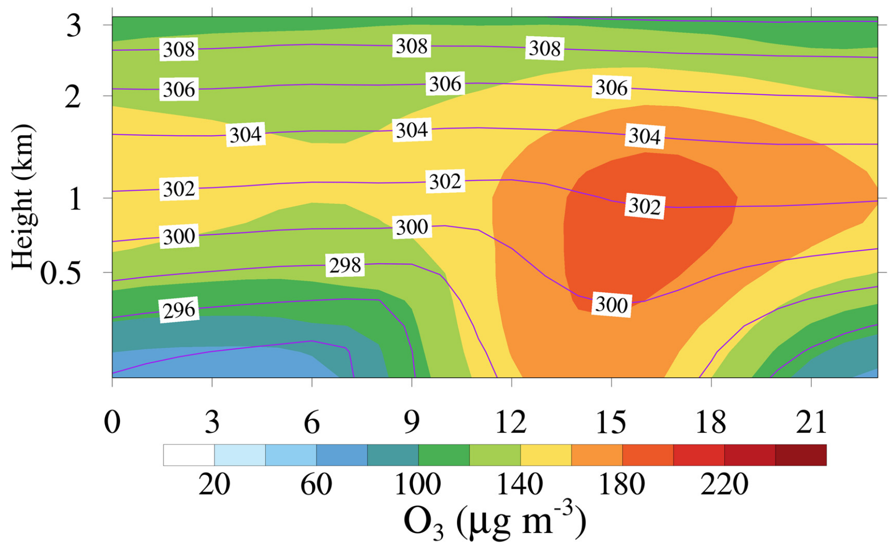


**Figure 8.** Temporal-vertical distribution of $O_3$ and potential temperature over the innermost domain in MODIS_noAH.

### 3.3.2 Sea and lake breezes

As shown in Figure 7a and b, in the areas where the local circulations meet the background dominant winds (the southeast wind), the converging airflows make $O_3$ concentrations higher than those in the surrounding areas. Furthermore, the typical local circulations in the central YRD are the sea and the lake breezes around the Tai Lake. In this study, the sea-breeze usually affected a wide area and lasted a long time, which may be related to the local background field since they are mostly in same direction, and it is difficult to separate the sea-breeze from the southeast wind. The sea-breeze was obvious around 14:00 LT and matured around 17:00 LT, and continuously transported high $O_3$ from coastal to the inland areas during this period (Figure 7b-d). Compared with the sea-breeze, the lake-breeze had a much smaller influencing area and a shorter duration. Around 11:00 LT, the lake-breeze was established. It reached its maximum intensity around 14:00 LT, and then disappeared sharply due to the predominant sea-breeze (Figure 7c). Both the sea and the lake breezes played important roles in the horizontal distributions of $O_3$ in the central YRD.

As the coastline is generally north-south (Figure 1b), the cross sections along line AB depicted in Figure 7a are illustrated to show representative example of the vertical structure of the sea breezes

https://doi.org/10.5194/acp-2021-619
Preprint. Discussion started: 17 August 2021




(Figure 9a-c). The sea-breeze below 500m had already developed by 11:00 LT. A sea-breeze front was found in front of Shanghai (~121.6°E), with a height of 1.5 km. The speed of sea-breeze increased around 14:00 LT, which can exceed 5 m $s^{-1}$. The intensified sea-breeze penetrated inland for a distance of 20-30 km, and the sea-breeze front (~121.4°E) lifted the boundary layer top over Shanghai up to ~2 km (Figure 9b). Strong sea-breeze swept across the central YRD around 17:00 LT, reducing the $O_3$ concentration near the surface in coastal areas. But the $O_3$ in the mixed layer still maintained a high level, which can result in an $O_3$-rich reservoir forming in the nocturnal residual layer (Figure 9c and 8). The penetration of sea-breeze front and its effect on surface $O_3$ can be also observed in other regions, such as the Pearl River Delta Region (You et al., 2019), Taiwan (Lin et al., 2007), the Athens basin (Mavrakou et al., 2012) and Paulo (Freitas et al., 2007).

As for the lake breezes, the cross sections along line CD (Figure 9d-f) and EF (Figure 9g-i) are given since the lake is usually inside the land so that the lake breezes can have different directions. The lake-breeze was established when the surface wind was weak by 11:00 LT (Figure 9d and g) though it was shallow at that time. Around 14:00 LT, the lake-breeze strengthened. The extension of the lake-breeze circulation zone can even reach up to 2 km in the vertical dimension. The offshore flow (~ 2 m $s^{-1}$) of the lake-breeze circulation transported high $O_3$ concentration from urban areas to the lake, while the onshore flow blew the $O_3$ back to urban areas (Figure 9e and h). Thus, the net effect is that the lake-breeze "accelerated" the vertical mixing in the boundary layer, resulting in high concentration of $O_3$ in the lakeside cities. The high surface $O_3$ concentration caused by the lake breezes has also been confirmed near other lakes, such as the Lake Michigan (Lennartson and Schwartz, 2002), the Great Lakes (Sills et al., 2011) and the Great Salt Lake (Blaylock et al., 2017). Finally, the lake-breeze was destroyed by the prevailing southwest wind by 17:00 LT.

https://doi.org/10.5194/acp-2021-619
Preprint. Discussion started: 17 August 2021


Atmospheric Chemistry and Physics
Discussions

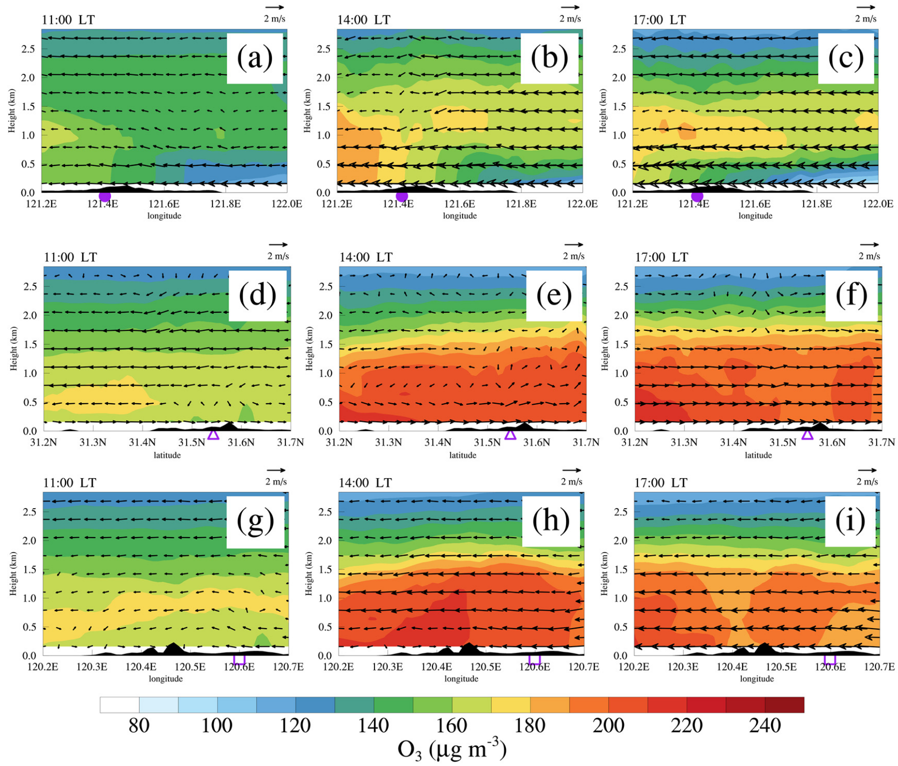


**Figure 9.** Vertical cross sections of $O_3$ and wind for sea-breeze at (a) 11:00, (b) 14:00 and (c) 17:00 LT along the line AB in Figure 7a. (d), (e) and (f) are the same as (a), (b) and (c), respectively, but for lake-breeze along the line CD in Figure 7a. (g), (h) and (i) are also the same as (a), (b) and (c), respectively, but for lake-breeze along the line EF in Figure 7a. The purple dots, triangles and rectangle represent the locations of Shanghai, Wuxi and Suzhou, respectively. The black shaded areas represent the terrain, and the terrain has been multiplied by a factor of 10 when plotting.

### 3.4 Impacts of land-surface forcing on meteorology and $O_3$

#### 3.4.1 The changes in horizontal direction

Figure 10 presents the spatial differences of the main factors, including $O_3$, $T_2$, PBLH and $WS_{10}$, between MODIS_noAH and USGS_noAH. Obviously, higher $O_3$ was produced in the MODIS_noAH, indicating that urban expansion will increase surface $O_3$ concentrations. The largest increment of $O_3$ occurred in the afternoon, with a value of 20 μg $m^{-3}$ around 17:00 LT in Changzhou. $T_2$ is directly affected by the land-atmosphere heat fluxes resulting from land-surface forcing. The

https://doi.org/10.5194/acp-2021-619
Preprint. Discussion started: 17 August 2021



spatial pattern of remarkable warming effect for $T_2$ was consistent with the urban-fraction change (Figure 2a and b), which is that the positive temperature anomaly often appeared in large cities and their surrounding areas. This positive forcing for $T_2$ is associated with the enhanced surface heating through upward sensible heat fluxes during the day. In megacities like Shanghai, $T_2$ can increase by 3 ℃. It should be noted that there was a confusing "false" warming at the junction of land and sea/lake, which was mainly caused by the different treatment of the MODIS-based and USGS land use classifications at the boundary conditions of land versus water (Figure 2a and b). The change in PBLH was similar to that in $T_2$, but it was less obvious after sunset around 20:00 LT. This is because that the warming up of $T_2$ can enhance the vertical air movement in the boundary layer and thereby increase the PBLH. The maximum positive change of PBLH reached up to 500 m in the urban areas at noon but downed to 100 m after sunset. The roughness of cities and forest is greater than that of cropland, so there was a decrease in $WS_{10}$ in the MODIS_noAH (Figure 9m-p), with a maximum decrease up to 1.5 m $s^{-1}$ in Hangzhou around 17:00 LT.

Atmospheric Chemistry and Physics Discussions

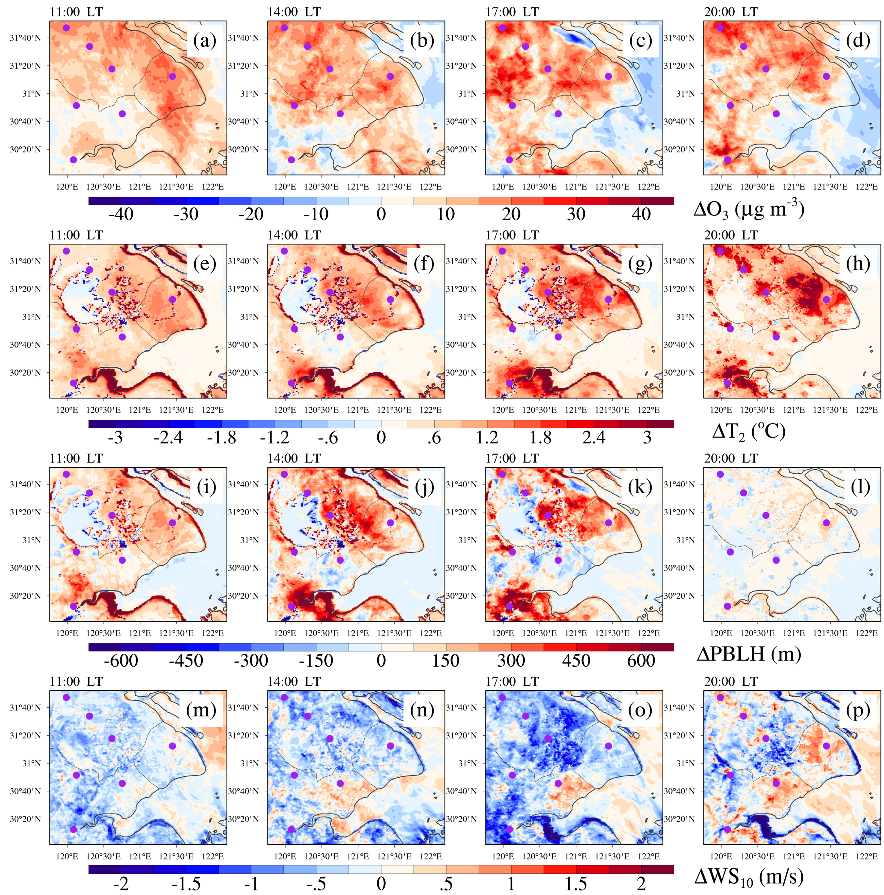


**Figure 10.** Horizontal distributions of the (a-d) $O_3$, (e-h) $T_2$, (i-l) PBLH and (m-p) $WS_{10}$ differences between MODIS_noAH and USGS_noAH (MODIS_noAH – USGS_noAH) at different times (11:00, 14:00, 17:00 and 20:00 LT) of the day. The purple dots represent the locations of cities (red dots in Figure 1b) in the innermost domain.

### 3.4.2 The changes in vertical direction

As shown in Figure 11a-c, the sea-breeze below 500 m increased by 1-2 m $s^{-1}$ due to the existence of the cities which enhanced the temperature contrast between the land and the sea. Strong turbulent mixing and updraft induced by the sea-breeze front promote the development of the urban boundary layer, contributing to elevated $O_3$ levels at surface in the city during the advance of the sea-breeze front inland (Figure 11a and b). When the sea-breeze matured around 17:00 LT, its transport effect reduced the surface $O_3$ concentration of the coastal cities (Figure 9c). However, this

https://doi.org/10.5194/acp-2021-619
Preprint. Discussion started: 17 August 2021



"removal" was weakened because the sea-breeze near the surface was slowed due to the rough urban surface. Finally, surface $O_3$ of about 10 μg $m^{-3}$ was left compared to the scenario without cities (Figure 11c).

As for the lake-breeze, it was also enhanced by 1-2 m $s^{-1}$ after the establishment because of the larger temperature contrast resulting from the cities, just like the sea-breeze (Figure 11e and h). And the life of the lake-breeze was extended to 17:00 LT (Figure 11f and i) when the city exists. Because the lake-breeze was conducive to the vertical mixing of the boundary layer and its onshore flow can blow high concentration of $O_3$ from the lake to the city (Sect. 3.3.2), the urban $O_3$ concentration will eventually increase, with a maximum of 30 μg $m^{-3}$ in Wuxi at 14:00 LT.

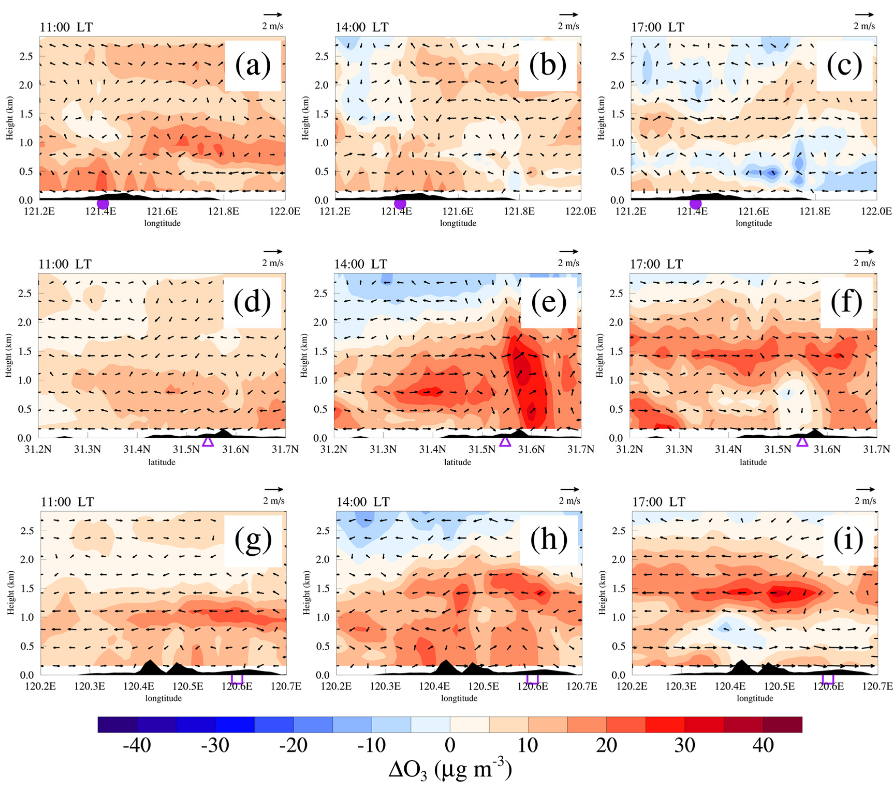


**Figure 11.** Same as Figure 9, but for the differences between MODIS_noAH and USGS_noAH (MODIS_noAH – USGS_noAH).

### 3.4.3 The mechanism of land-surface forcing modulating $O_3$

Land-surface forcing plays an important role in the evolution of $O_3$ by changing the local meteorology (meteorological factors and local circulations). Changing land-surface forcing from USGS to MODIS leads to an increase in $T_2$ by maximum 3 °C, an increase in PBLH by maximum 500 m and a decrease in $WS_{10}$ by maximum 1.5 m $s^{-1}$ in the YRD, which is comparable to those in the BTH region (Yu et al., 2012), the PRD region (Li et al., 2014) and the National Capital Region of India (Sati and Mohan, 2017). And these changes are particularly evident in and around cities. The elevated air temperature is conducive to the photochemical production of $O_3$, and the well-developed boundary layer favors the vertical mixing of $O_3$ (Figure 12), which increases the $O_3$ concentration near the surface by maximum 20 μg $m^{-3}$. This change magnitude in $O_3$ is consistent with the findings reported in Seoul (Ryu et al., 2013b) and Southern California (Li et al., 2019). Local circulations (the sea and the lake breezes) are also influenced by the land-surface forcing, chiefly from the urban expansion as the most significant land-surface forcing in the YRD comes from urban expansion over the past few decades. For the coastal cities, like Shanghai, the larger temperature contrast induced by cities enhances the sea-breeze below 500 m. As the sea-breeze front moves inland, it can induce stronger upward air flow that deepens the boundary layer. Thus, high $O_3$ concentration in the middle of boundary layer can be more easily transported to the surface. However, the movement of the sea-breeze is slowed due to the rough urban surface after the sea-breeze matures. The removal of the sea-breeze is then weakened and the surface $O_3$ increases by 10 μg $m^{-3}$. The similar response of the sea breezes to urban expansion as well as its impact on $O_3$ has been also reported in the PRD region (You et al., 2019) and Paulo (Freitas et al., 2007). For the lakeside cities, like Wuxi and Suzhou, the lifetime of the lake breezes is extended to the afternoon due to the existence of the city. The offshore flow of the lake-breeze transports high $O_3$ concentration in the middle of the boundary layer from the land to the lake, while the onshore flow brings the $O_3$ back to the land, which accelerates the vertical mixing of $O_3$ and can increase the surface $O_3$ by even 30 μg $m^{-3}$. High surface $O_3$ appears when the lake breezes have been established can also be observed in the Greater Toronto Area (Wentworth et al., 2015) and the Lake Michigan (Abdi-Oskouei et al., 2020).

https://doi.org/10.5194/acp-2021-619
Preprint. Discussion started: 17 August 2021

Atmospheric Chemistry and Physics
Discussions

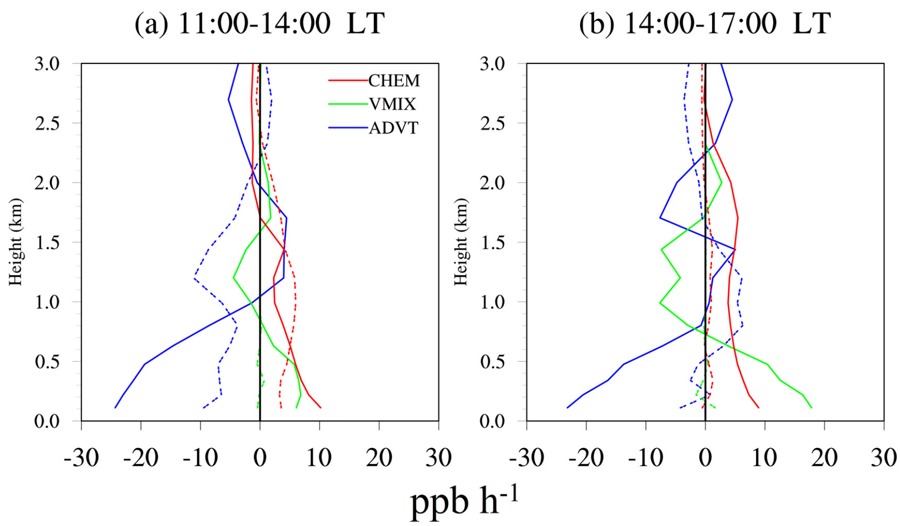


**Figure 12.** Vertical profiles of the changes in individual processes between MODIS_noAH and USGS_noAH (MODIS_noAH – USGS_noAH) at (a) 11:00-14:00 LT and (b) 14:00-17:00 LT over Shanghai (solid lines) and Wuxi (dashed lines). CHEM (in red), VMIX (in green) and ADVT (in blue) represent gas-phase chemical reactions, turbulent mixing and advection transport, respectively.

### 3.5 Impacts of anthropogenic heat on meteorology and $O_3$

#### 3.5.1 Horizontal changes

Compared with land-surface forcing, the changes caused by AH are much smaller (Figure 13). Furthermore, these changes in meteorology and $O_3$ mainly occur in and around cities as there are more AH emissions in these areas (Figure 3). Surface $O_3$ concentration increased in the urban areas by about 4 μg m$^{-3}$ in the simulation with adding AH, and this phenomenon was clearer after sunset (Figure 13d). By adding more surface sensible heat into the atmosphere, the AH fluxes can lead to an increase in $T_2$ of 0.2 °C during the day, with the typical value of 0.42 °C in Shanghai. Vertical air movement in the boundary layer can be enhanced by the warming up of the surface air temperature, thereby the PBLH will increase as well. According to the simulations, the PBLH increased by about 75 m in the urban areas. With regards to $WS_{10}$, it increased by about 0.3 m s$^{-1}$ in the urban areas, which is contrary to the decrease in $WS_{10}$ caused by land-surface forcing (Sect. 3.4.1). This is ascribed to the strengthened urban-breeze circulations induced by the AH fluxes, which is mentioned in previous studies (Ryu et al., 2013a, b; Xie et al., 2016a, b).

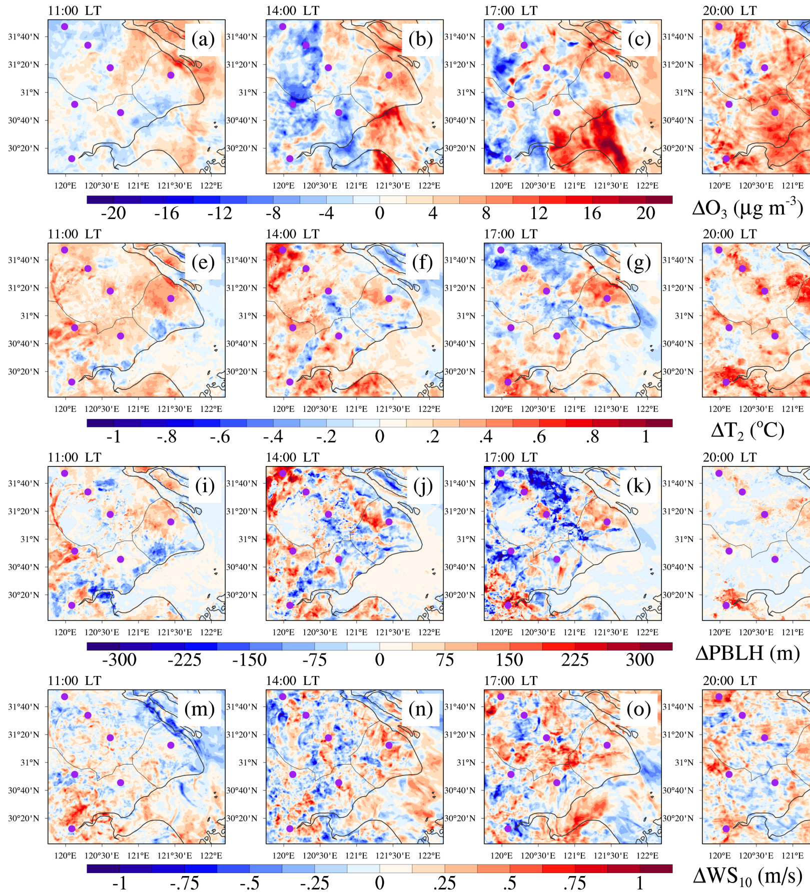


**Figure 13.** Same as Figure 10, but for the differences between MODIS_withAH and MODIS_noAH (MODIS_withAH – MODIS_noAH).

### 3.5.2 Vertical changes

The phenomenon that cities are almost always warmer than their surroundings is known as the urban heat island (UHI), and the difference between the urban and the rural surface energy balance can further initiate the UHI circulation. It is clearly seen that an enhanced UHI circulation driven by AH appeared in the megacity Shanghai around 14:00 LT (Figure 14b). This circulation extended horizontally 20-30 km from the city center to the urban edge, and vertically to nearly 2 km from the ground to the top of the urban boundary layer. Under this condition, there was a small increase (4~6

https://doi.org/10.5194/acp-2021-619
Preprint. Discussion started: 17 August 2021

Atmospheric Chemistry and Physics Discussions

$\mu g\ m^{-3}$) in $O_3$ concentrations in the low boundary layer. However, for the lakeside cities, the enhanced UHI circulation was not visibly noticed, and the $O_3$ concentration in urban areas was reduced on average, with a maximum of 16 $\mu g\ m^{-3}$ in Wuxi around 14:00 LT (Figure 14e). The lower $O_3$ concentration may be affected by the increased wind on the lake (Figure 13), which was beneficial to the diffusion and dilution processes. Furthermore, it seems that AH has a limited effect on local circulations, regardless of the sea or lake breeze, though it play an important role in the urban-breeze circulations. In our simulation cases, AH does not continuously and significantly affect any branch of the local circulations like the land-surface forcing.

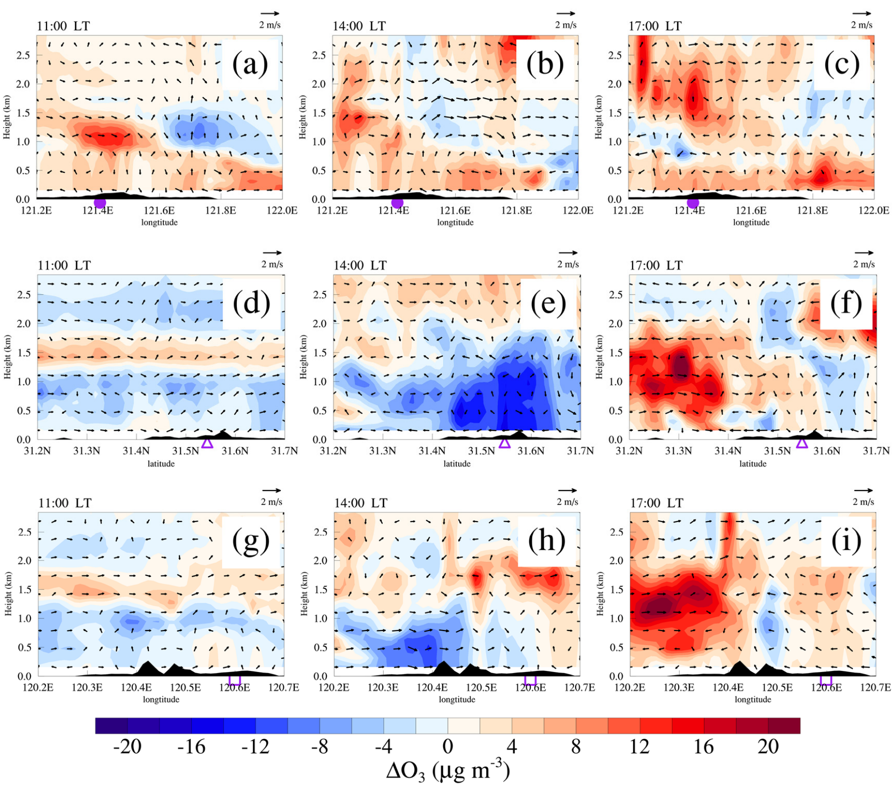


**Figure 14.** Same as Figure 8, but for the differences between MODIS_withAH and MODIS_noAH (MODIS_withAH – MODIS_noAH).

### 3.5.3 The mechanism of anthropogenic heat modulating $O_3$

https://doi.org/10.5194/acp-2021-619
Preprint. Discussion started: 17 August 2021




AH and land-surface forcing play different roles in meteorology and $O_3$. AH allows the atmosphere to reserve more energy via the additional sensible heat fluxes, which increases $T_2$ by about 0.2 °C. Higher temperature is conducive to the development of the convective boundary layer and can induce stronger upward air movement, which rises the PBLH by about 75 m. In the convective boundary layer, the atmosphere is associated with turbulent motions, and is unstable. Together with the urban-breeze circulations enhanced by AH, $WS_{10}$ can increase by 0.3 m $s^{-1}$. These findings are comparable to the values estimated in other cities all around the world, such as Philadelphia in the United States (Fan and Sailor, 2005), Winnipeg in Canada (Ferguson and Woodbury, 2007), Berlin in German (Menberg et al., 2013) and Tokyo in Japan (Dhakal and Hanaki, 2002). It is noteworthy that the abovementioned changes mainly appear in large cities and their surrounding areas, where AH emission centers are located. And these changes eventually caused an increase in surface $O_3$ concentration by about 4 μg $m^{-3}$. Additionally, though AH can play an important role in urban-breeze circulations, it may not be powerful enough to affect the local circulations such as the sea and the lake breezes.

## 4 Summary and conclusions

Land-surface forcing related to the urban expansion and AH release from human activities can change the meteorology (meteorological factors and local circulations) and thereby affect $O_3$ air quality in and around cities. In this study, the YRD region, a highly urbanized place with sever $O_3$ pollution and complex geography, is selected to discuss this issue. Firstly, we briefly describe the general characteristics of $O_3$ pollution in the YRD based on the surface observations. Secondly, we simulate a representative case using WRF-chem and evaluate the model performance by comparing with the observational data. Finally, the response of meteorology as well as $O_3$ to land-surface forcing and AH are investigated from the model results. The main findings are listed as below:

(1) Regional $O_3$ pollution occurs frequently in the YRD (~ 26 times per year). Like other regions, these $O_3$ pollution episodes mainly occur in warm season (April to October) under calm conditions characterized by high temperature (over 20 °C), low relative humidity (less than 80%), light wind (less than 3 m $s^{-1}$) and shallow cloud cover (less than 5). In this case, the local circulations induced by thermal differentiation tend to develop and will have an important impact on the distribution of $O_3$.

https://doi.org/10.5194/acp-2021-619
Preprint. Discussion started: 17 August 2021




(2) By updating the land-use data from USGS to MODIS, we find an increase in $T_2$ by maximum 3 °C, an increase in PBLH by maximum 500 m and a decrease in $WS_{10}$ by maximum 1.5 m $s^{-1}$ in the YRD, which is comparable to those in the BTH region (Yu et al., 2012), the PRD region (Li et al., 2014) and the National Capital Region of India (Sati and Mohan, 2017). The higher temperature and PBLH elevate the $O_3$ level by maximum 20 μg $m^{-3}$ via the photochemical and the vertical mixing processes, respectively. For changes in local circulations, the sea-breeze below 500 m is enhanced due to larger temperature contrast induced by the urban expansion. During the advance of the sea-breeze front inland, the upward air flow in front of the front is conducive to the vertical mixing of $O_3$. When the sea-breeze is well formed in the late afternoon, further progression inland is stalled on account of the rough urban surface. The transport of high $O_3$ from coastal to the inland areas is weakened and thereby $O_3$ can be 10 μg $m^{-3}$ higher in the case with cities than without. The similar results have been also reported in the Paulo (Freitas et al., 2007) and the PRD region (You et al., 2019). With respect to the lake breezes, its lifetime will be extended from the noon to the afternoon because of the urban expansion. Since the net effect of the lake-breeze is to accelerate the vertical mixing in the boundary layer, the surface $O_3$ can increase as much as 30 μg $m^{-3}$ influenced by the lake-breeze. Similar phenomenon also be observed in the Greater Toronto Area (Wentworth et al., 2015) and the Lake Michigan (Abdi-Oskouei et al., 2020).

(3) The changes caused by AH are different from land-surface forcing. These changes are relatively small and mainly appear around the cities where there are large AH emissions. Through regulating the land-atmosphere heat fluxes, $O_3$, $T_2$, PBLH and $WS_{10}$ increases by about 4 μg $m^{-3}$, 0.2 °C, 75 m and 0.3 m $s^{-1}$ under the effect of the additional sensible heat fluxes induced by AH. The magnitudes of these changes are consistent with the values estimated in other cities all around the world, including Philadelphia in the United States (Fan and Sailor, 2005), Winnipeg in Canada (Ferguson and Woodbury, 2007), Tokyo in Japan (Dhakal and Hanaki, 2002) and Berlin in German (Menberg et al., 2013). Additionally, our results show that AH may have a quite limited impact on local circulations, such as the sea and the lake breezes. But the urban-breeze circulations in and around big cities are sensitive to AH inputs, which can further affect the urban air pollutants.

Estimating the impacts of land-surface forcing and AH on urban climate and air quality is a complex but necessary issue as these two are important manifestations of urbanization. Although our study only focuses on the YRD region, most of the results can be supported by previous studies that conducted in other region around the world. Thus, our work may provide valuable insight into the formation of $O_3$ pollution in those rapidly developing regions with unique geographical features.

***Data Availability Statement.***

Air quality monitoring data were acquired from a mirror of data from the official NEMC real-time publishing platform (https://quotsoft.net/air/). Meteorological data were issued by the NCDC (ftp://ftp.ncdc.noaa.gov/pub/data/noaa/isd-lite/). The FNL meteorological data were acquired from NCEP (https://doi.org/10.5065/D6M043C6/). These data can be downloaded for free as long as you agree to the official instructions.

***Author contributions.***

CZ and MX had the original ideas, designed the research, collected the data and prepared the original draft. CZ did the numerical simulations and carried out the data analysis. MX acquired financial support for the project leading to this publication.

***Acknowledgements.***

This work was supported by the National Key Research and Development Program of China (2018YFC0213502, 2018YFC1506404). We are grateful to MEPC for the air quality monitoring data, to NCDC for the meteorological data, to NCEP for global final analysis fields and to Tsinghua University for the MEIC inventories. The numerical calculations have been done on the Blade cluster system in the High Performance Computing and Massive Data Center (HPC&MDC) of School of Atmospheric Sciences, Nanjing University. We also thank the constructive comments and suggestions from the anonymous reviewers.

**References**

Abdi-Oskouei, M., Carmichael, G., Christiansen, M., Ferrada, G., Roozitalab, B., Sobhani, N., Wade, K., Czarnetzki, A., Pierce, R. B., Wagner, T., and Stanier, C.: Sensitivity of Meteorological Skill to Selection of WRF-Chem Physical Parameterizations and Impact on Ozone Prediction During the Lake Michigan Ozone Study (LMOS), J Geophys Res-Atmos, 125, 2020.

Blaylock, B. K., Horel, J. D., and Crosman, E. T.: Impact of Lake Breezes on Summer Ozone

https://doi.org/10.5194/acp-2021-619
Preprint. Discussion started: 17 August 2021



Concentrations in the Salt Lake Valley, Journal of Applied Meteorology and Climatology, 56, 353-370, 2017.

Buchholz, S., Junk, J., Krein, A., Heinemann, G., and Hoffmann, L.: Air pollution characteristics associated with mesoscale atmospheric patterns in northwest continental Europe, Atmospheric Environment, 44, 5183-5190, 10.1016/j.atmosenv.2010.08.053, 2010.

Chameides, W., and Walker, J. C. G.: A photochemical theory of tropospheric ozone, Journal of Geophysical Research, 78, 8751-8760, 10.1029/JC078i036p08751, 1973.

Chen, F., and Dudhia, J.: Coupling an advanced land surface-hydrology model with the Penn State-NCAR MM5 modeling system. Part II: Preliminary model validation, Monthly Weather Review, 129, 587-604, 2001.

Chen, S. H., and Sun, W. Y.: A one-dimensional time dependent cloud model, J Meteorol Soc Jpn, 80, 99-118, 2002.

Crosman, E. T., and Horel, J. D.: Sea and Lake Breezes: A Review of Numerical Studies, Boundary-Layer Meteorology, 137, 1-29, 10.1007/s10546-010-9517-9, 2010.

Dhakal, S., and Hanaki, K.: Improvement of urban thermal environment by managing heat discharge sources and surface modification in Tokyo, Energ Buildings, 34, 13-23, 2002.

Ding, A., Wang, T., Zhao, M., Wang, T., and Li, Z.: Simulation of sea-land breezes and a discussion of their implications on the transport of air pollution during a multi-day ozone episode in the Pearl River Delta of China, Atmospheric Environment, 38, 6737-6750, 10.1016/j.atmosenv.2004.09.017, 2004.

Ding, A. J., Fu, C. B., Yang, X. Q., Sun, J. N., Zheng, L. F., Xie, Y. N., Herrmann, E., Nie, W., Petäjä, T., Kerminen, V. M., and Kulmala, M.: Ozone and fine particle in the western Yangtze River Delta: an overview of 1 yr data at the SORPES station, Atmospheric Chemistry and Physics, 13, 5813-5830, 10.5194/acp-13-5813-2013, 2013.

Fan, H. L., and Sailor, D. J.: Modeling the impacts of anthropogenic heating on the urban climate of Philadelphia: a comparison of implementations in two PBL schemes, Atmospheric Environment, 39, 73-84, 2005.

Fast, J. D., Gustafson, W. I., Easter, R. C., Zaveri, R. A., Barnard, J. C., Chapman, E. G., Grell, G. A., and Peckham, S. E.: Evolution of ozone, particulates, and aerosol direct radiative forcing in the vicinity of Houston using a fully coupled meteorology-chemistry-aerosol model, J

Geophys Res-Atmos, 111, 2006.

Ferguson, G., and Woodbury, A. D.: Urban heat island in the subsurface, Geophysical Research Letters, 34, 2007.

Flanner, M. G.: Integrating anthropogenic heat flux with global climate models, Geophysical Research Letters, 36, n/a-n/a, 10.1029/2008gl036465, 2009.

Freitas, E. D., Rozoff, C. M., Cotton, W. R., and Dias, P. L. S.: Interactions of an urban heat island and sea-breeze circulations during winter over the metropolitan area of Sao Paulo, Brazil, Boundary-Layer Meteorology, 122, 43-65, 2007.

Friedl, M. A., Sulla-Menashe, D., Tan, B., Schneider, A., Ramankutty, N., Sibley, A., and Huang, X.: MODIS Collection 5 global land cover: Algorithm refinements and characterization of new datasets, Remote Sensing of Environment, 114, 168-182, 10.1016/j.rse.2009.08.016, 2010.

Gao, D., Xie, M., Chen, X., Wang, T. J., Liu, J., Xu, Q., Mu, X. Y., Chen, F., Li, S., Zhuang, B. L., Li, M. M., Zhao, M., and Ren, J. Y.: Systematic classification of circulation patterns and integrated analysis of their effects on different ozone pollution levels in the Yangtze River Delta Region, China, Atmospheric Environment, 242, 2020.

Gong, P., Liu, H., Zhang, M., Li, C., Wang, J., Huang, H., Clinton, N., Ji, L., Li, W., Bai, Y., Chen, B., Xu, B., Zhu, Z., Yuan, C., Ping Suen, H., Guo, J., Xu, N., Li, W., Zhao, Y., Yang, J., Yu, C., Wang, X., Fu, H., Yu, L., Dronova, I., Hui, F., Cheng, X., Shi, X., Xiao, F., Liu, Q., and Song, L.: Stable classification with limited sample: transferring a 30-m resolution sample set collected in 2015 to mapping 10-m resolution global land cover in 2017, Science Bulletin, 64, 370-373, 10.1016/j.scib.2019.03.002, 2019.

Grell, G. A., and Dévényi, D.: A generalized approach to parameterizing convection combining ensemble and data assimilation techniques, Geophysical Research Letters, 29, 38-31-38-34, 10.1029/2002gl015311, 2002.

Grell, G. A., Peckham, S. E., Schmitz, R., McKeen, S. A., Frost, G., Skamarock, W. C., and Eder, B.: Fully coupled "online" chemistry within the WRF model, Atmospheric Environment, 39, 6957-6975, 10.1016/j.atmosenv.2005.04.027, 2005.

Guenther, A., Karl, T., Harley, P., Wiedinmyer, C., Palmer, P. I., and Geron, C.: Estimates of global terrestrial isoprene emissions using MEGAN (Model of Emissions of Gases and Aerosols from Nature), Atmospheric Chemistry and Physics, 6, 3181-3210, 2006.

https://doi.org/10.5194/acp-2021-619
Preprint. Discussion started: 17 August 2021




Hong, S. Y., Noh, Y., and Dudhia, J.: A new vertical diffusion package with an explicit treatment of entrainment processes, Monthly Weather Review, 134, 2318-2341, 2006.

Hu, J., Li, Y., Zhao, T., Liu, J., Hu, X.-M., Liu, D., Jiang, Y., Xu, J., and Chang, L.: An important mechanism of regional O<sub>3</sub> transport for summer smog over the Yangtze River Delta in eastern China, Atmospheric Chemistry and Physics, 18, 16239-16251, 10.5194/acp-18-16239-2018, 2018.

Jacob, D. J., and Winner, D. A.: Effect of climate change on air quality, Atmospheric Environment, 43, 51-63, 10.1016/j.atmosenv.2008.09.051, 2009.

Jerrett, M., Burnett, R. T., Pope, C. A., Ito, K., Thurston, G., Krewski, D., Shi, Y. L., Calle, E., and Thun, M.: Long-Term Ozone Exposure and Mortality., New Engl J Med, 360, 1085-1095, 2009.

Jimenez, P. A., and Dudhia, J.: Improving the Representation of Resolved and Unresolved Topographic Effects on Surface Wind in the WRF Model, Journal of Applied Meteorology and Climatology, 51, 300-316, 2012.

Kim, H.-J., and Wang, B.: Sensitivity of the WRF model simulation of the East Asian summer monsoon in 1993 to shortwave radiation schemes and ozone absorption, Asia-Pacific Journal of Atmospheric Sciences, 47, 167-180, 10.1007/s13143-011-0006-y, 2011.

Lennartson, G. J., and Schwartz, M. D.: The lake breeze-ground-level ozone connection in eastern Wisconsin: A climatological perspective, International Journal of Climatology, 22, 1347-1364, 2002.

Li, M., Song, Y., Huang, X., Li, J., Mao, Y., Zhu, T., Cai, X., and Liu, B.: Improving mesoscale modeling using satellite-derived land surface parameters in the Pearl River Delta region, China, Journal of Geophysical Research: Atmospheres, 119, 6325-6346, 10.1002/2014jd021871, 2014.

Li, Y., Zhang, J., Sailor, D. J., and Ban-Weiss, G. A.: Effects of urbanization on regional meteorology and air quality in Southern California, Atmospheric Chemistry and Physics, 19, 4439-4457, 10.5194/acp-19-4439-2019, 2019.

Li, K., Jacob, D. J., Shen, L., Lu, X., De Smedt, I., and Liao, H.: Increases in surface ozone pollution in China from 2013 to 2019: anthropogenic and meteorological influences, Atmospheric Chemistry and Physics, 20, 11423-11433, 10.5194/acp-20-11423-2020, 2020.

Liao, Z., Gao, M., Sun, J., and Fan, S.: The impact of synoptic circulation on air quality and pollution-related human health in the Yangtze River Delta region, Sci Total Environ, 607-608, 838-846, 10.1016/j.scitotenv.2017.07.031, 2017.

Lin, C. H., Lai, C. H., Wu, Y. L., Lin, P. H., and Lai, H. C.: Impact of sea breeze air masses laden with ozone on inland surface ozone concentrations: A case study of the northern coast of Taiwan, J Geophys Res-Atmos, 112, 2007.

Liu, M., and Tian, H.: China's land cover and land use change from 1700 to 2005: Estimations from high-resolution satellite data and historical archives, Global Biogeochemical Cycles, 24, n/a-n/a, 10.1029/2009gb003687, 2010.

Loveland, T. R., Reed, B. C., Brown, J. F., Ohlen, D. O., Zhu, Z., Yang, L., and Merchant, J. W.: Development of a global land cover characteristics database and IGBP DISCover from 1 km AVHRR data, International Journal of Remote Sensing, 21, 1303-1330, 10.1080/014311600210191, 2000.

Lu, X., Hong, J., Zhang, L., Cooper, O. R., Schultz, M. G., Xu, X., Wang, T., Gao, M., Zhao, Y., and Zhang, Y.: Severe Surface Ozone Pollution in China: A Global Perspective, Environmental Science & Technology Letters, 5, 487-494, 10.1021/acs.estlett.8b00366, 2018.

Mavrakou, T., Philippopoulos, K., and Deligiorgi, D.: The impact of sea breeze under different synoptic patterns on air pollution within Athens basin, Science of the Total Environment, 433, 31-43, 2012.

Menberg, K., Bayer, P., Zosseder, K., Rumohr, S., and Blum, P.: Subsurface urban heat islands in German cities, Sci Total Environ, 442, 123-133, 10.1016/j.scitotenv.2012.10.043, 2013.

Miao, Y., Hu, X.-M., Liu, S., Qian, T., Xue, M., Zheng, Y., and Wang, S.: Seasonal variation of local atmospheric circulations and boundary layer structure in the Beijing-Tianjin-Hebei region and implications for air quality, Journal of Advances in Modeling Earth Systems, 7, 1602-1626, 10.1002/2015ms000522, 2015.

Mlawer, E. J., Taubman, S. J., Brown, P. D., Iacono, M. J., and Clough, S. A.: Radiative transfer for inhomogeneous atmospheres: RRTM, a validated correlated-k model for the longwave, Journal of Geophysical Research: Atmospheres, 102, 16663-16682, 10.1029/97jd00237, 1997.

Oke, T. R.; Mills, G.; Christen, A.; Voogt, J. A. Urban Climates; Cambridge University Press: Cambridge, 2017.

Ryu, Y. H., Baik, J. J., Kwak, K. H., Kim, S., and Moon, N.: Impacts of urban land-surface forcing on ozone air quality in the Seoul metropolitan area, Atmospheric Chemistry and Physics, 13, 2177-2194, 10.5194/acp-13-2177-2013, 2013b.

Ryu, Y.-H., Baik, J.-J., and Lee, S.-H.: Effects of anthropogenic heat on ozone air quality in a megacity, Atmospheric Environment, 80, 20-30, 10.1016/j.atmosenv.2013.07.053, 2013a.

Sailor, D. J.: A review of methods for estimating anthropogenic heat and moisture emissions in the urban environment, International Journal of Climatology, 31, 189-199, 10.1002/joc.2106, 2011.

Sati, A. P., and Mohan, M.: The impact of urbanization during half a century on surface meteorology based on WRF model simulations over National Capital Region, India, Theoretical and Applied Climatology, 134, 309-323, 2017.

Schell, B., Ackermann, I. J., Hass, H., Binkowski, F. S., and Ebel, A.: Modeling the formation of secondary organic aerosol within a comprehensive air quality model system, J Geophys Res-Atmos, 106, 28275-28293, 2001.

Shao, M., Tang, X. Y., Zhang, Y. H., and Li, W. J.: City clusters in China: air and surface water pollution, Front Ecol Environ, 4, 353-361, 2006.

Sills, D. M. L., Brook, J. R., Levy, I., Makar, P. A., Zhang, J., and Taylor, P. A.: Lake breezes in the southern Great Lakes region and their influence during BAQS-Met 2007, Atmospheric Chemistry and Physics, 11, 7955-7973, 10.5194/acp-11-7955-2011, 2011.

Stockwell, W. R., Middleton, P., Chang, J. S., and Tang, X. Y.: The 2nd Generation Regional Acid Deposition Model Chemical Mechanism for Regional Air-Quality Modeling, J Geophys Res-Atmos, 95, 16343-16367, 1990.

Van Dingenen, R., Dentener, F. J., Raes, F., Krol, M. C., Emberson, L., and Cofala, J.: The global impact of ozone on agricultural crop yields under current and future air quality legislation, Atmospheric Environment, 43, 604-618, 10.1016/j.atmosenv.2008.10.033, 2009.

Wang, T., Xue, L., Brimblecombe, P., Lam, Y. F., Li, L., and Zhang, L.: Ozone pollution in China: A review of concentrations, meteorological influences, chemical precursors, and effects, Sci Total Environ, 575, 1582-1596, 10.1016/j.scitotenv.2016.10.081, 2017.

Wang, Y., Gao, W., Wang, S., Song, T., Gong, Z., Ji, D., Wang, L., Liu, Z., Tang, G., Huo, Y., Tian, S., Li, J., Li, M., Yang, Y., Chu, B., Petäjä, T., Kerminen, V.-M., He, H., Hao, J., Kulmala, M., Wang, Y., and Zhang, Y.: Contrasting trends of $PM_{2.5}$ and surface-ozone concentrations in China from 2013 to 2017, National Science Review, 7, 1331-1339, 10.1093/nsr/nwaa032, 2020.

Wentworth, G. R., Murphy, J. G., and Sills, D. M. L.: Impact of lake breezes on ozone and nitrogen oxides in the Greater Toronto Area, Atmospheric Environment, 109, 52-60, 10.1016/j.atmosenv.2015.03.002, 2015.

Worden, H. M., Bowman, K. W., Worden, J. R., Eldering, A., and Beer, R.: Satellite measurements of the clear-sky greenhouse effect from tropospheric ozone, Nature Geoscience, 1, 305-308, 2008.

Xie, M., Zhu, K., Wang, T., Yang, H., Zhuang, B., Li, S., Li, M., Zhu, X., and Ouyang, Y.: Application of photochemical indicators to evaluate ozone nonlinear chemistry and pollution control countermeasure in China, Atmospheric Environment, 99, 466-473, 10.1016/j.atmosenv.2014.10.013, 2014.

Xie, M., Liao, J., Wang, T., Zhu, K., Zhuang, B., Han, Y., Li, M., and Li, S.: Modeling of the anthropogenic heat flux and its effect on regional meteorology and air quality over the Yangtze River Delta region, China, Atmospheric Chemistry and Physics, 16, 6071-6089, 10.5194/acp-16-6071-2016, 2016a.

Xie, M., Zhu, K., Wang, T., Feng, W., Gao, D., Li, M., Li, S., Zhuang, B., Han, Y., Chen, P., and Liao, J.: Changes in regional meteorology induced by anthropogenic heat and their impacts on air quality in South China, Atmospheric Chemistry and Physics, 16, 15011-15031, 10.5194/acp-16-15011-2016, 2016b.

Xie, M., Shu, L., Wang, T.-j., Liu, Q., Gao, D., Li, S., Zhuang, B.-l., Han, Y., Li, M.-m., and Chen, P.-l.: Natural emissions under future climate condition and their effects on surface ozone in the Yangtze River Delta region, China, Atmospheric Environment, 150, 162-180, 10.1016/j.atmosenv.2016.11.053, 2017.

You, C., Fung, J. C. H., and Tse, W. P.: Response of the Sea Breeze to Urbanization in the Pearl River Delta Region, Journal of Applied Meteorology and Climatology, 58, 1449-1463, 2019.

Young, P. J., Archibald, A. T., Bowman, K. W., Lamarque, J. F., Naik, V., Stevenson, D. S., Tilmes, S., Voulgarakis, A., Wild, O., Bergmann, D., Cameron-Smith, P., Cionni, I., Collins, W. J., Dalsøren, S. B., Doherty, R. M., Eyring, V., Faluvegi, G., Horowitz, L. W., Josse, B., Lee, Y. H., MacKenzie, I. A., Nagashima, T., Plummer, D. A., Righi, M., Rumbold, S. T., Skeie, R. B., Shindell, D. T., Strode, S. A., Sudo, K., Szopa, S., and Zeng, G.: Pre-industrial to end 21st century projections of tropospheric ozone from the Atmospheric Chemistry and Climate Model

Intercomparison Project (ACCMIP), Atmospheric Chemistry and Physics, 13, 2063-2090, 10.5194/acp-13-2063-2013, 2013.

Yu, M., Carmichael, G. R., Zhu, T., and Cheng, Y.: Sensitivity of predicted pollutant levels to urbanization in China, Atmospheric Environment, 60, 544-554, 10.1016/j.atmosenv.2012.06.075, 2012.

Zhan, C.-c., Xie, M., Fang, D.-x., Wang, T.-j., Wu, Z., Lu, H., Li, M.-m., Chen, P.-l., Zhuang, B.-l., Li, S., Zhang, Z.-q., Gao, D., Ren, J.-y., and Zhao, M.: Synoptic weather patterns and their impacts on regional particle pollution in the city cluster of the Sichuan Basin, China, Atmospheric Environment, 208, 34-47, 10.1016/j.atmosenv.2019.03.033, 2019.

Zhan, C., Xie, M., Huang, C., Liu, J., Wang, T., Xu, M., Ma, C., Yu, J., Jiao, Y., Li, M., Li, S., Zhuang, B., Zhao, M., and Nie, D.: Ozone affected by a succession of four landfall typhoons in the Yangtze River Delta, China: major processes and health impacts, Atmospheric Chemistry and Physics, 20, 13781-13799, 10.5194/acp-20-13781-2020, 2020.

Zhan, C., Xie, M., Liu, J., Wang, T., Xu, M., Chen, B., Li, S., Zhuang, B., and Li, M.: Surface Ozone in the Yangtze River Delta, China: A Synthesis of Basic Features, Meteorological Driving Factors, and Health Impacts, Journal of Geophysical Research: Atmospheres, 126, 10.1029/2020jd033600, 2021.

Zhang, N., Zhu, L., and Zhu, Y.: Urban heat island and boundary layer structures under hot weather synoptic conditions: A case study of Suzhou City, China, Advances in Atmospheric Sciences, 28, 855-865, 10.1007/s00376-010-0040-1, 2011.

Zhang, H., Wang, Y., Hu, J., Ying, Q., and Hu, X. M.: Relationships between meteorological parameters and criteria air pollutants in three megacities in China, Environ Res, 140, 242-254, 10.1016/j.envres.2015.04.004, 2015.

Zhu, B., Kang, H., Zhu, T., Su, J., Hou, X., and Gao, J.: Impact of Shanghai urban land surface forcing on downstream city ozone chemistry, Journal of Geophysical Research: Atmospheres, 120, 4340-4351, 10.1002/2014jd022859, 2015.